

Electron-Phonon Coupling and the Metalization of Solid Helium at Terapascal Pressures

Bartomeu Monserrat,^{1,*} N. D. Drummond,² Chris J. Pickard,³ and R. J. Needs¹

¹*TCM Group, Cavendish Laboratory, University of Cambridge,
J. J. Thomson Avenue, Cambridge CB3 0HE, United Kingdom*

²*Department of Physics, Lancaster University, Lancaster LA1 4YB, United Kingdom*

³*Department of Physics and Astronomy, University College London,
Gower Street, London WC1E 6BT, United Kingdom*

(Dated: March 25, 2022)

Solid He is studied in the pressure and temperature ranges 1–40 TPa and 0–10,000 K using first-principles methods. Anharmonic vibrational properties are calculated within a self-consistent field framework, including the internal and free energies, density-pressure relation, stress tensor, thermal expansion, and the electron-phonon coupling renormalization of the electronic band gap. We find that an accurate description of electron-phonon coupling requires us to use a non-perturbative approach. The metalization pressure of 32.9 TPa at 0 K is larger than found previously. The vibrational effects are large; for example at $P = 30$ TPa the band gap is increased by 2.8 eV by electron-phonon coupling and a further 0.1 eV by thermal expansion compared to the static value. The implications of the calculated metalization pressure for the cooling of white dwarfs are discussed.

PACS numbers: 63.20.Ry, 71.38.-k, 62.50.p

Helium (He) is the second most abundant element in the Universe after hydrogen and one of the most important components of stellar bodies such as giant gaseous planets, main-sequence stars, and white dwarf (WD) stars. The large value of the first excitation energy of atomic He of 19.82 eV leads to a high metalization pressure for the solid phase, of the order of tens of terapascals. Calculations of the phase diagram of He [1, 2] indicate that, in the terapascal pressure range, it remains solid up to temperatures of around 8,000 K. He is therefore expected to be found in the solid state in the outer layers of cool WDs.

The vast majority of the stars in the Universe become WDs in the final stages of their evolution, with the gravitational attraction towards the center being balanced by the electron degeneracy pressure of the high-density core. The lack of a continuous energy source means that WDs cool down until reaching thermodynamic equilibrium with their surroundings, eventually becoming black dwarfs. An understanding of the cooling process [3] is essential when calculating the ages of observed WDs, which are widely used within cosmochronology [4, 5] to date stellar clusters and galaxies, and hence to provide bounds on the age of the Universe.

The cores of WDs are largely isothermal due to the high thermal conductivity of degenerate electrons. Hence the cooling rate is mainly determined by the outer layers, which are composed of hydrogen, He, or a mixture of both. In this context the insulator-metal transition in solid He is central because energy transport from the degenerate core is dominated by electron transport through metallic He in the deeper layers, and by photon transport through insulating He in the outermost region [6].

Recent work has focused on the study of the metal-

ization pressure of He in the solid and fluid states [6–11]. In the solid state [6], static-lattice electronic structure calculations using both the diffusion Monte Carlo (DMC) many-body wave function technique [12, 13] and the GW approximation of many-body perturbation theory [14] have shown that standard generalized gradient approximations [15] to density functional theory (DFT) [16, 17] substantially underestimate band gaps. In the fluid state [7], the effects of electron-phonon coupling lead to a strong temperature dependence of the metalization pressure. The effects of temperature on the metalization transition in the solid state remain an open question.

He is the second lightest element and therefore the amplitudes of the nuclear vibrations are expected to be large and possibly to present anharmonic behavior. Recent advances in the treatment of anharmonicity from first-principles make the incorporation of these effects feasible [18–23]. For the determination of band gaps in the solid state, both electron-phonon coupling and thermal expansion are important [24–26]. Studying the effects of electron-phonon coupling on the band gaps of solids from first principles has only recently become possible [22, 27–30]. In this paper, we combine the first-principles calculation of anharmonicity, electron-phonon coupling and thermal expansion to study the vibrational corrections to the thermal band gap of solid He and hence determine an accurate value for the metalization pressure including the effects of temperature.

We use the principal-axes approximation [22, 31] to the Born-Oppenheimer energy surface, considering independent phonon terms and pairwise phonon-phonon interactions. The resulting Schrödinger equation for the nuclear coordinates is solved within the vibrational self-consistent field (VSCF) framework [22, 32] for the vibra-

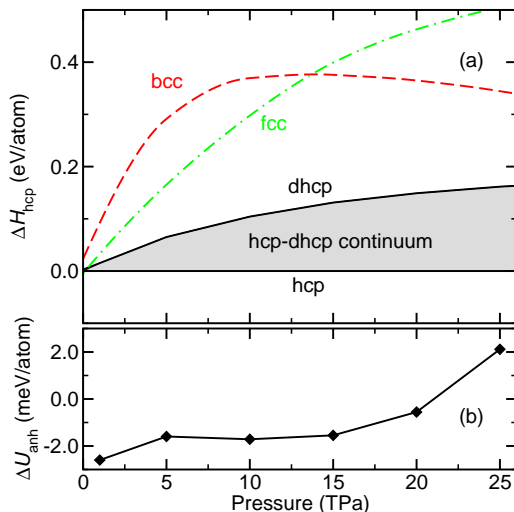


FIG. 1. (color online) (a) Enthalpy ΔH_{hcp} with respect to the hcp phase of the closed-packed phases described at the static DFT level. (b) Anharmonic energy correction ΔU_{anh} to the harmonic energy of the hcp phase at zero temperature.

tional anharmonic energy E_{S} and wave function $|\Phi^{\text{S}}(\mathbf{Q})\rangle$ in state S , where \mathbf{Q} is a collective phonon coordinate. We use second-order perturbation theory to go beyond the mean-field formulation. We then calculate phonon expectation values of a general operator $\hat{O}(\mathbf{Q})$ at zero and finite temperature T according to

$$\langle \hat{O}(\mathbf{Q}) \rangle = \frac{1}{\mathcal{Z}} \sum_{\text{S}} \langle \Phi^{\text{S}}(\mathbf{Q}) | \hat{O}(\mathbf{Q}) | \Phi^{\text{S}}(\mathbf{Q}) \rangle e^{-E_{\text{S}}/k_{\text{B}}T}, \quad (1)$$

where \mathcal{Z} is the partition function and k_{B} is Boltzmann's constant. This expectation value can be calculated by writing the operator $\hat{O}(\mathbf{Q})$ within a principal axes representation like that for the energy [22], or non-perturbatively by sampling phase space according to the nuclear density [28, 30]. The first method is approximate, but the description is in terms of individual phonons, permitting direct access to the underlying physical processes. The second method can in principle lead to accurate numerical results, but the underlying physical mechanisms are obscured. Here we will use a combination of both methods to obtain a full picture of the effects of electron-phonon coupling on the band gap of solid He. We note that the use of DFT to calculate electron-phonon corrections to band gaps is reasonable, as the usual band-gap underestimation cancels in the difference between the static gap and the phonon-renormalized gap [29].

We have solved the electronic Schrödinger equation to map the Born-Oppenheimer energy surface within plane-wave DFT [16, 17] as implemented in the CASTEP code [33]. We have used ultrasoft pseudopotentials [34] with core radii of 0.212 Å, which require an energy cutoff of 2800 eV, and Monkhorst-Pack [35] \mathbf{k} -point grids of spacing $2\pi \times 0.04 \text{ \AA}^{-1}$. These parameters lead to energy differ-

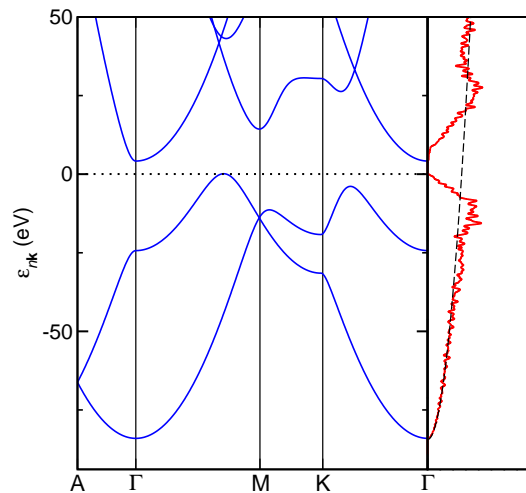


FIG. 2. (color online) Electronic band structure (blue) and density of states (red, on right-hand-side of figure) of hcp He at 10 TPa. The dashed black line is the density of states of a free electron gas of the same density as He.

ences converged to within 10^{-4} eV per atom and stresses to within 10^{-1} GPa. All calculations were performed with the Perdew-Burke-Ernzerhof [15] generalized gradient approximation density functional. We solved the vibrational Schrödinger equation within the VSCF formalism by expanding the wave function in a basis of simple harmonic oscillator (SHO) eigenstates. This basis is defined from a quadratic fit to the Born-Oppenheimer energy surface calculated within the principal axes approximation rather than from the harmonic approximation. We have included 100 SHO states for each phonon degree of freedom, which leads to converged results.

The phase diagram of solid He at low pressures is well-characterized, and the hexagonal close-packed (hcp) structure with a c/a ratio close to ideal has been found to be stable up to at least 58 GPa [36]. It is usually assumed that He remains in the solid hcp phase up to high pressures and temperatures, but this does not seem to have been tested in detail. Furthermore, at the highest pressures it is expected to be in a body-centered cubic (bcc) phase. We have therefore performed searches at 10 and 20 TPa using the *ab initio* random structure searching (AIRSS) method [37, 38] to find low-enthalpy crystal structures of He with 12 or fewer atoms per cell. We have calculated the harmonic vibrational free energy of the most competitive phases in the temperature range 0–10,000 K, and several phases were found that were lower in free energy than the face-centered cubic (fcc) and the bcc phases, but none of them were more stable than hcp. In Fig. 1 we show the static lattice enthalpy ΔH_{hcp} with respect to the hcp enthalpy of the closed-packed phases as a function of pressure. The difference in enthalpy between these closed-packed phases varies with pressure, which shows that the electronic structures of the phases,

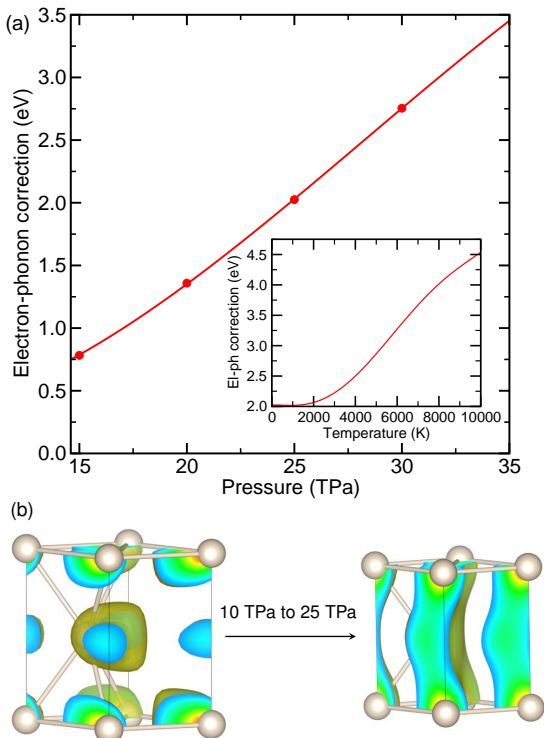


FIG. 3. (color online) (a) ZP electron-phonon correction to the thermal band gap of hcp solid He as a function of pressure. The inset shows the temperature dependence of the electron-phonon correction at a pressure of $P = 25$ TPa. (b) Squared Kohn-Sham eigenstate corresponding to the CBM at 10 TPa and 25 TPa, using a R-G-B color scale with red corresponding to high density and blue to low density. We have removed the regions of lowest density for clarity.

as well as packing considerations, are important in determining the relative enthalpies. The hcp and double hexagonal closed-packed (dhcp) structures are the two end members of a series of structures which differ in the stacking of layers. The energies per layer of these structures vary continuously with the fraction of stacking faults present.

We have also calculated the anharmonic free energy contribution ΔF_{anh} for the hcp structure (see Fig. 1). For example, at 10 TPa and zero temperature the harmonic energy is 686.9 meV/atom and the anharmonic correction is -1.7 meV/atom due to the independent phonon term, and it is further renormalized by $+1.1$ meV/atom due to the two-body phonon term. At $T = 5,000$ K, the harmonic free energy is 75.0 meV/atom, and the anharmonic correction is -5.2 meV/atom. At 25 TPa and zero temperature the harmonic energy is 903.0 meV/atom and the anharmonic correction is only 2.1 meV/atom, whereas at $T = 5,000$ K, the harmonic free energy is 466.6 meV/atom and the anharmonic correction is 6.3 meV/atom. Second-order perturbation theory does not change these results within the reported precision,

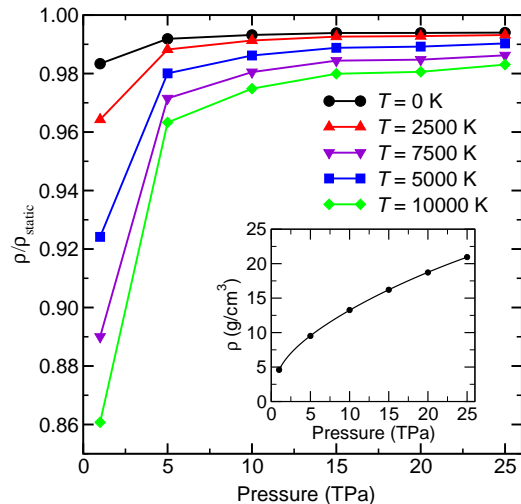


FIG. 4. (color online) Density-pressure-temperature phase diagram of solid hcp He. At a given external pressure, the density ρ is renormalized with respect to the static-lattice density ρ_{static} at that pressure. The inset shows the density-pressure relation at $T = 0$ K, including the effects of ZP motion.

demonstrating the accuracy of the mean-field approximation. These anharmonic corrections, albeit larger than in heavier systems such as diamond [22], remain remarkably small and have no discernible effect on the relative stability of the phases considered. Furthermore, the ratio of the anharmonic to quasi-harmonic vibrational free energy decreases with increasing pressure, which suggests that anharmonicity becomes less important for the energetics of He at high pressures.

The band structure and density of states of solid hcp He at 10 TPa are shown in Fig. 2. The density of states of the occupied bands is very close to that of a free electron gas at the same density, reflecting the free-electron nature of high-pressure He. The valence band maximum (VBM) is located along the symmetry line joining the Γ and M points, while the conduction band minimum (CBM) is located at the Γ point, as observed experimentally at lower pressures [39]. We have evaluated the expression in Eq. (1), with \hat{O} becoming the difference between the CBM and the VBM, both within a principal axes representation and non-perturbatively to investigate the band-gap renormalization of solid hcp He due to electron-phonon coupling [40]. Figure 3 shows the pressure dependence of the zero-point (ZP) electron-phonon correction to the thermal band gap of hcp solid He calculated non-perturbatively. A second calculation of the same quantity with a principal axes representation of $E_g(\mathbf{Q})$ gives information about the underlying physical mechanisms. The out-of-plane modes of the hcp lattice couple strongly to the electronic bands and their effect is to open the band gap. This coupling increases with pressure, and it leads to the behavior shown in Fig. 3. This

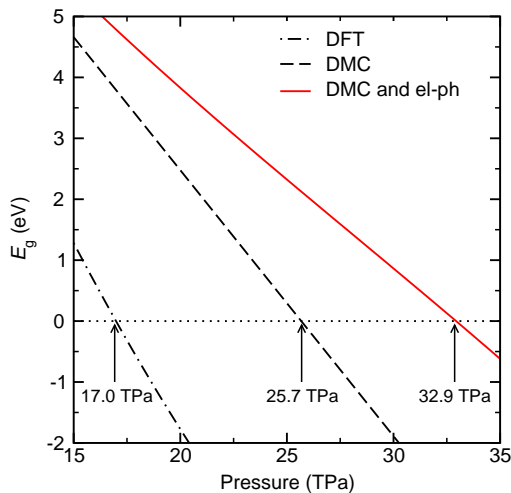


FIG. 5. (color online) Thermal band gap E_g of solid hcp He as a function of pressure, calculated by evaluating the difference between the CBM and the VBM (even when the difference is negative). The static gap results correspond to DFT calculations (dashed-dotted black line) and DMC calculations (dashed black line) taken from Ref. [6]. The band gap including the effects of electron-phonon coupling and thermal expansion added to the DMC results is shown at $T = 0$ K (red solid line).

can be further understood by analyzing the Kohn-Sham eigenstates corresponding to the VBM and the CBM (shown in Fig. 3). At lower pressure these eigenstates are localized around the atomic sites, but as pressure increases they delocalize in the interplane direction, hence increasing the coupling with the out-of-plane modes. We emphasize that the non-perturbative calculation of the renormalization of the band gap due to electron-phonon coupling leads to quantitatively different results to the perturbative approach. Terms beyond lowest-order perturbation theory are found to be crucial for calculating the correction to the band gap [41]. The magnitude of the band gap renormalization is, as far as we are aware, amongst the largest reported, similar only to that found in high-pressure solid hydrogen [42].

To investigate thermal expansion we have calculated the vibrational stress tensor at finite temperatures using the formalism described in Ref. [22]. The vibrational stress tensor is diagonal, with similar in-plane and out-of-plane stresses, leading to an isotropic volume expansion. Figure 4 shows the density-pressure relation at five different temperatures, including the full vibrational effects. Both ZP and finite-temperature expansions are more significant at lower pressures. This occurs because the system stiffens with increasing pressure (see the inset of Fig. 4), and although the vibrational stress tensor is larger at higher pressures, the resulting density change is smaller. At $P = 25$ TPa, the ZP correction to the volume at $T = 0$ K opens the gap by 0.105 eV, and the thermal expansion at $T = 5,000$ K opens the gap by 0.216 eV.

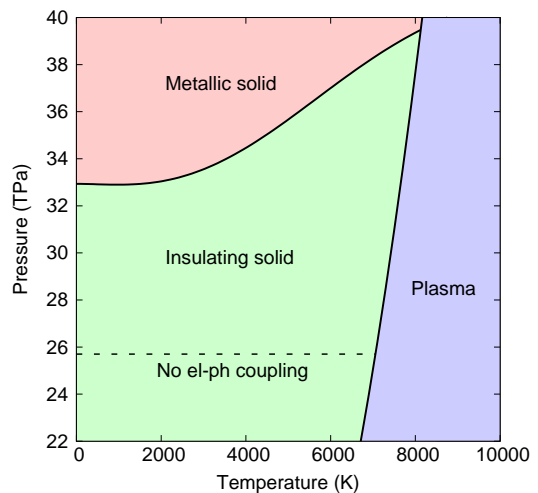


FIG. 6. (color online) Phase diagram of He at the pressure-temperature range relevant for cool WDs. The black dashed line is the insulator-metal transition predicted in Ref. [6]. The solid-plasma transition is taken from Ref. [2].

Combining the effects of electron-phonon coupling and thermal expansion on the band gap, we calculate the pressure dependence of the thermal band gap of solid He near metalization, as shown in Fig. 5. The static-lattice DFT value has been calculated using the PBE functional. The static-lattice DMC results are those reported in Ref. [6], where GW calculations lead to results matching those from DMC calculations. The curve including electron-phonon coupling and ZP expansion at zero temperature leads to a metalization pressure of 32.9 TPa, significantly higher than the static-lattice value.

The renormalization of the band gap due to lattice vibrations near the metalization pressure is in the range 3.0–4.0 eV for temperatures in the range 0–5,000 K. These values represent a quantitative change to the static lattice value of the same order of magnitude as the electron-correlation correction to DFT [6]. Furthermore, our results are the first to describe the temperature-dependence of the transition. The authors of Ref. [6] considered the effects of temperature on the electronic band gap within path integral Monte Carlo [43], and concluded that they are negligible. We have come to a significantly different conclusion on this issue, but there is not enough information in Ref. [6] to be able to make a more detailed comparison. From the considerations above and the data of Ref. [2], we can construct the phase diagram of He at the pressures and temperatures relevant for cool WDs as shown in Fig. 6.

In conclusion, we have presented first-principles calculations of the phase stability, electron-phonon coupling, and thermal expansion in solid He for a range of pressures and temperatures. We have shown that the thermodynamically stable phase of solid He is hcp for the pressure range 1–30 TPa and temperature range 0–10,000 K, in-

cluding anharmonic energies at the mean-field level. The second-order perturbation theory used to go beyond the VSCF approximation gives a negligible correction, suggesting that the mean field energy is accurate. The effects of electron-phonon coupling on the band gap are substantial and several times larger than the effects of thermal expansion. A perturbative approach is not accurate here, and it is important to use a non-perturbative scheme, as we have done. We have determined the metal-insulator transition of solid He to be at 32.9 TPa at $T = 0$ K, which may be compared with the value 25.7 TPa obtained in Ref. [6] at the static-lattice level.

The increase in the metalization pressure of solid He when the effects of electron-phonon coupling and thermal expansion are included implies that the interiors of WDs have a metallic He layer that is thinner than the one predicted by a purely electronic treatment, and a correspondingly thicker insulating layer, where heat transport is dominated by photons. The temperature dependence of the metalization pressure indicates that, as WDs cool, the thickness of the metallic layer increases at the expense of the insulating layer. These results suggest that white dwarf stars may be older than previously thought.

Financial support was provided by the Engineering and Physical Sciences Research Council (UK). The calculations were performed on the Cambridge High Performance Computing Service facility.

* bm418@cam.ac.uk

- [1] D. A. Young, A. K. McMahan, and M. Ross, *Phys. Rev. B*, **24**, 5119 (1981).
- [2] A. Förster, T. Kahlbaum, and W. Ebeling, *Laser Part. Beams*, **10**, 253 (1992).
- [3] F. D'Antona and I. Mazzitelli, *Annu. Rev. Astron. Astrophys.*, **28**, 139 (1990).
- [4] D. E. Winget, C. J. Hansen, J. Liebert, H. M. van Horn, G. Fontaine, R. E. Nather, S. O. Kepler, and D. Q. Lamb, *Astrophys. J. Lett.*, **315**, L77 (1987).
- [5] T. D. Oswalt, J. A. Smith, M. A. Wood, and P. Hintzen, *Nature*, **382**, 692 (1996).
- [6] S. A. Khairallah and B. Militzer, *Phys. Rev. Lett.*, **101**, 106407 (2008).
- [7] L. Stixrude and R. Jeanloz, *Proc. Natl. Acad. Sci. USA*, **105**, 11071 (2008).
- [8] P. M. Kowalski, S. Mazevet, D. Saumon, and M. Challacombe, *Phys. Rev. B*, **76**, 075112 (2007).
- [9] P. M. Celliers, P. Loubeyre, J. H. Eggert, S. Brygoo, R. S. McWilliams, D. G. Hicks, T. R. Boehly, R. Jeanloz, and G. W. Collins, *Phys. Rev. Lett.*, **104**, 184503 (2010).
- [10] F. Soubiran, S. Mazevet, C. Winisdoerffer, and G. Chabrier, *Phys. Rev. B*, **86**, 115102 (2012).
- [11] J. M. McMahon, M. A. Morales, C. Pierleoni, and D. M. Ceperley, *Rev. Mod. Phys.*, **84**, 1607 (2012).
- [12] D. M. Ceperley and B. J. Alder, *Phys. Rev. Lett.*, **45**, 566 (1980).
- [13] W. M. C. Foulkes, L. Mitas, R. J. Needs, and G. Rajagopal, *Rev. Mod. Phys.*, **73**, 33 (2001).
- [14] F. Aryasetiawan and O. Gunnarsson, *Rep. Prog. Phys.*, **61**, 237 (1998).
- [15] J. P. Perdew, K. Burke, and M. Ernzerhof, *Phys. Rev. Lett.*, **77**, 3865 (1996).
- [16] P. Hohenberg and W. Kohn, *Phys. Rev.*, **136**, B864 (1964).
- [17] W. Kohn and L. J. Sham, *Phys. Rev.*, **140**, A1133 (1965).
- [18] P. Souvatzis, O. Eriksson, M. I. Katsnelson, and S. P. Rudin, *Phys. Rev. Lett.*, **100**, 095901 (2008).
- [19] I. Errea, B. Rousseau, and A. Bergara, *Phys. Rev. Lett.*, **106**, 165501 (2011).
- [20] O. Hellman, I. A. Abrikosov, and S. I. Simak, *Phys. Rev. B*, **84**, 180301 (2011).
- [21] N. Antolin, O. D. Restrepo, and W. Windl, *Phys. Rev. B*, **86**, 054119 (2012).
- [22] B. Monserrat, N. D. Drummond, and R. J. Needs, *Phys. Rev. B*, **87**, 144302 (2013).
- [23] I. Errea, M. Calandra, and F. Mauri, [arxiv:1305.7123](https://arxiv.org/abs/1305.7123) (2013).
- [24] M. Cardona and M. L. W. Thewalt, *Rev. Mod. Phys.*, **77**, 1173 (2005).
- [25] P. B. Allen and V. Heine, *J. Phys. C*, **9**, 2305 (1976).
- [26] P. B. Allen and M. Cardona, *Phys. Rev. B*, **23**, 1495 (1981).
- [27] R. D. King-Smith, R. J. Needs, V. Heine, and M. J. Hodgson, *Europhys. Lett.*, **10**, 569 (1989).
- [28] R. Ramírez, C. P. Herrero, and E. R. Hernández, *Phys. Rev. B*, **73**, 245202 (2006).
- [29] F. Giustino, S. G. Louie, and M. L. Cohen, *Phys. Rev. Lett.*, **105**, 265501 (2010).
- [30] C. E. Patrick and F. Giustino, *Nat. Commun.*, **4**, 2006 (2013).
- [31] J. O. Jung and R. B. Gerber, *J. Chem. Phys.*, **105**, 10332 (1996).
- [32] J. M. Bowman, *J. Chem. Phys.*, **68**, 608 (1978).
- [33] S. J. Clark, M. D. Segall, C. J. Pickard, P. J. Hasnip, M. I. J. Probert, K. Refson, and M. C. Payne, *Z. Kristallogr.*, **220**, 567 (2005).
- [34] D. Vanderbilt, *Phys. Rev. B*, **41**, 7892 (1990).
- [35] H. J. Monkhorst and J. D. Pack, *Phys. Rev. B*, **13**, 5188 (1976).
- [36] P. Loubeyre, R. LeToullec, J. P. Pinceaux, H. K. Mao, J. Hu, and R. J. Hemley, *Phys. Rev. Lett.*, **71**, 2272 (1993).
- [37] C. J. Pickard and R. J. Needs, *Phys. Rev. Lett.*, **97**, 045504 (2006).
- [38] C. J. Pickard and R. J. Needs, *J. Phys. Condens. Matter*, **23**, 053201 (2011).
- [39] H. K. Mao, E. L. Shirley, Y. Ding, P. Eng, Y. Q. Cai, P. Chow, Y. Xiao, J. Shu, R. J. Hemley, C. Kao, and W. L. Mao, *Phys. Rev. Lett.*, **105**, 186404 (2010).
- [40] Supercells containing 54 atoms are used for all reported calculations. Tests with supercells containing up to 250 atoms show a convergence of the band gap corrections within 0.2 eV, leading to an uncertainty of 0.4 TPa in the metallization pressure. For the non-perturbative calculations, a total of 1,000 sampling points have been used at each pressure and temperature, leading to statistical error bars smaller than the reported accuracy.
- [41] B. Monserrat, G. J. Conduit, and R. J. Needs, [arxiv:1308.3483](https://arxiv.org/abs/1308.3483) (2013).
- [42] M. A. Morales, J. M. McMahon, C. Pierleoni, and D. M. Ceperley, *Phys. Rev. B*, **87**, 184107 (2013).
- [43] D. M. Ceperley, *Rev. Mod. Phys.*, **67**, 279 (1995).